Linking the Tropical Northern Hemisphere Pattern to the Pacific Warm Blob and Atlantic Cold Blob

Yu-Chiao Liang, Jin-Yi Yu, and Eric S. Saltzman

Department of Earth System Science, University of California, Irvine, Irvine, California

Fan Wang

Institute of Oceanography, Chinese Academy of Science, Qingdao, China

ABSTRACT

During 2013–15, prolonged near-surface warming in the northeastern Pacific was observed and has been referred to as the Pacific warm blob. Here, statistical analyses are conducted to show that the generation of the Pacific blob is closely related to the tropical Northern Hemisphere (TNH) pattern in the atmosphere. When the TNH pattern stays in its positive phase for extended periods of time, it generates prolonged blob events primarily through anomalies in surface heat fluxes and secondarily through anomalies in wind-induced ocean advection. Five prolonged ($\geq$24 months) blob events are identified during the past six decades (1948–2015), and the TNH–blob relationship can be recognized in all of them. Although the Pacific decadal oscillation and El Niño can also induce an arc-shaped warming pattern near the Pacific blob region, they are not responsible for the generation of Pacific blob events. The essential feature of Pacific blob generation is the TNH-forced Gulf of Alaska warming pattern. This study also finds that the atmospheric circulation anomalies associated with the TNH pattern in the North Atlantic can induce SST variability akin to the so-called Atlantic cold blob, also through anomalies in surface heat fluxes and wind-induced ocean advection. As a result, the TNH pattern serves as an atmospheric conducting pattern that connects some of the Pacific warm blob and Atlantic cold blob events. This conducting mechanism has not previously been explored.

1. Introduction

The term "Pacific warm blob" (Bond et al. 2015) was coined to refer to the remarkably warm water mass in the northeastern (NE) Pacific that persisted during 2013–15. At its peaks during the winter of 2014 and summer of 2015, the positive sea surface temperature (SST) anomalies in the warming region reached as high as 2°–3°C and penetrated as deep as 180 m below the ocean surface (Bond et al. 2015; Hu et al. 2017). This patch of warm water then propagated from the Gulf of Alaska toward the coastal regions, resulting in an arc-shaped warming off the North American coasts during the following winter (Amaya et al. 2016; Di Lorenzo and Mantua 2016; Gentemann et al. 2017). This Pacific warm blob event exerted pervasive impacts on coastal ecosystems, North American climate, and air quality. Examples of the Pacific blob impacts include a profound species range shift in the Gulf of Alaska (Medred 2014), dramatic changes in the marine productivity in the NE Pacific (Whitney 2015; Siedlecki et al. 2016), a delay in the onset of the upwelling off California coasts (Peterson et al. 2015; Zaba and Rudnick 2016), and altered springtime air temperatures (Bond et al. 2015) and ozone concentration (Jaffe and Zhang 2017) in the Pacific Northwest of the United States. Intensive efforts have been expended on attempts to understand the causes of this unusual marine heatwave phenomenon (Di Lorenzo and Mantua 2016).

Studies of the 2013–15 Pacific warm blob event have largely agreed that the warming was generated by an unusually persistent ridge system in the atmosphere over the NE Pacific region (Seager et al. 2014; Swain et al. 2014; Wang et al. 2014; Bond et al. 2015; Hartmann 2015; Seager et al. 2015; Amaya et al. 2016; Di Lorenzo and Mantua 2016; Swain et al. 2016; Hu et al. 2017). This anomalous high-pressure system can induce clockwise surface wind anomalies that work against the prevailing surface westerlies to reduce local surface evaporation and weaken cold ocean advection in the NE Pacific, giving rise to the Pacific warm blob (Bond et al. 2015).

Corresponding author: Jin-Yi Yu, jyyu@uci.edu

Atmospheric circulation patterns that have an anomaly center close to or encompassing the location of this anomalous ridge are possibly involved in the generation of the Pacific blob. A list of such patterns includes at least the Pacific–North American (PNA) pattern (Wallace and Gutzler 1981), the North Pacific Oscillation (NPO) pattern (Rogers 1981), and the tropical Northern Hemisphere (TNH) pattern (Mo and Livezey 1986). Among them, the NPO and PNA patterns have been invoked to explain how the Pacific blob evolved from the Gulf of Alaska (GOA) warming pattern to the arc-shaped (ARC) warming pattern during the 2013–15 event (Amaya et al. 2016; Di Lorenzo et al. 2016; Di Lorenzo and Mantua 2016). The possible role of the TNH pattern has not been examined in past Pacific blob studies.

Concurrent with the 2013–15 Pacific warm blob event, a region of persistently below-normal SSTs was observed in the North Atlantic. This cooling event is referred to as the Atlantic cold blob (Henson 2016) or the Atlantic warming hole (Rahmstorf et al. 2015) to emphasize the fact that this is the most prominent area in global oceans that has cooled in the face of a prevailing warming trend in global oceans (Henson 2016; Robson et al. 2016). The Atlantic cold blob was also suggested to affect downstream European climate (Duchez et al. 2016). Several mechanisms have been proposed to explain the generation of the Atlantic cold blob, including atmospheric forcing associated with the North Atlantic Oscillation (NAO; Delworth et al. 2016; Yeager et al. 2016), an ocean circulation change linked to the Atlantic meridional overturning circulation (AMOC; Rahmstorf et al. 2015; Robson et al. 2016; Duchez et al. 2016), and the melting of the Greenland ice sheet (Schmittner et al. 2016). The general perspective of the scientific community at this point is to consider the Atlantic and Pacific blobs as two separate phenomena that are driven by different mechanisms. However, the coincident occurrence of the 2013–15 Atlantic cold blob and Pacific warm blob events raises the possibility that some fraction of such Atlantic and Pacific blob events may be linked by atmospheric circulation patterns that have a cross-basin structure (i.e., from North Pacific to North Atlantic). If such a pattern exists, it can serve as a mechanism to induce climate connectivity between the North Pacific and North Atlantic sectors, some of which may be manifested as the co-occurrence of Pacific and Atlantic blob events.

In this study, we analyze reanalysis products to show that the atmospheric circulation pattern associated with the generation of the Pacific blob closely resembles the TNH pattern. We discuss the mechanisms through which the TNH pattern generates the Pacific warm blob (section 3) and the roles of the Pacific decadal oscillation (PDO) and El Niño–Southern Oscillation (ENSO) play in the evolution of the Pacific warm blob (section 4). The possible connection between the Pacific blob and the Atlantic blob events is examined (section 5). Section 6 summarizes the findings in this study and their implications for the Pacific–Atlantic climate connectivity and discusses the possible mechanisms that give rise to the TNH pattern.

2. Datasets and methods

In this study, the SST data are from the Hadley Centre Sea Ice and Sea Surface Temperature dataset (Rayner et al. 2003). Atmospheric wind fields, geopotential heights, and sea level pressure (SLP) are from the National Centers for Environmental Prediction (NCEP)–National Center for Atmospheric Research (NCAR) reanalysis dataset (Kalnay et al. 1996). Mixed layer temperatures, surface heat fluxes, and ocean currents are from the NCEP Global Ocean Data Assimilation System (GODAS, Behringer et al. 1998). GODAS products can differ from real observations due to the assimilation framework used that includes model simulation results (Xue et al. 2011; Kumar and Hu 2012). However, they are capable of capturing the general features of surface oceanic conditions and are used here to study the blob generation. Anomalies during the analysis period (1948–2015) are defined as deviations from the 1981–2010 climatology. The linear trends are removed from these fields before performing the analyses. Similar results are obtained when these trends are retained (not shown).

Several indices were used in the analyses. Following Bond et al. (2015), the Pacific blob index is calculated as the SST anomalies averaged within the box bounded by 40°–50°N and 150°–135°W. This blob box encompasses the ''point'' used in Amaya et al. (2016) to delineate the Pacific blob warming feature and is also covered by the two boxes used in the blob study of Di Lorenzo and Mantua (2016) to depict SST pattern shifts during 2014–15. The Atlantic cold blob index is defined as minus one (e.g., −1) times the SST anomalies averaged within the box bounded by 44°–56°N and 45°–25°W, which is close to the SST cooling region studied by Rahmstorf et al. (2015). This index is used to characterize the Atlantic cold blob variability. The Niño-3.4 index is used to represent ENSO activity. The PDO and PNA indices are obtained from NOAA's Earth System Research Laboratory and Climate Prediction Center. The NPO index is defined as the second-leading principal component of SLP anomalies over the North Pacific sector following Yu and Kim (2011).

The TNH pattern has been identified as an important atmospheric circulation mode of the Northern Hemisphere (NH) winter season in many studies (Esbensen 1984; Mo 1985; Mo and Livezey 1986; Barnston and
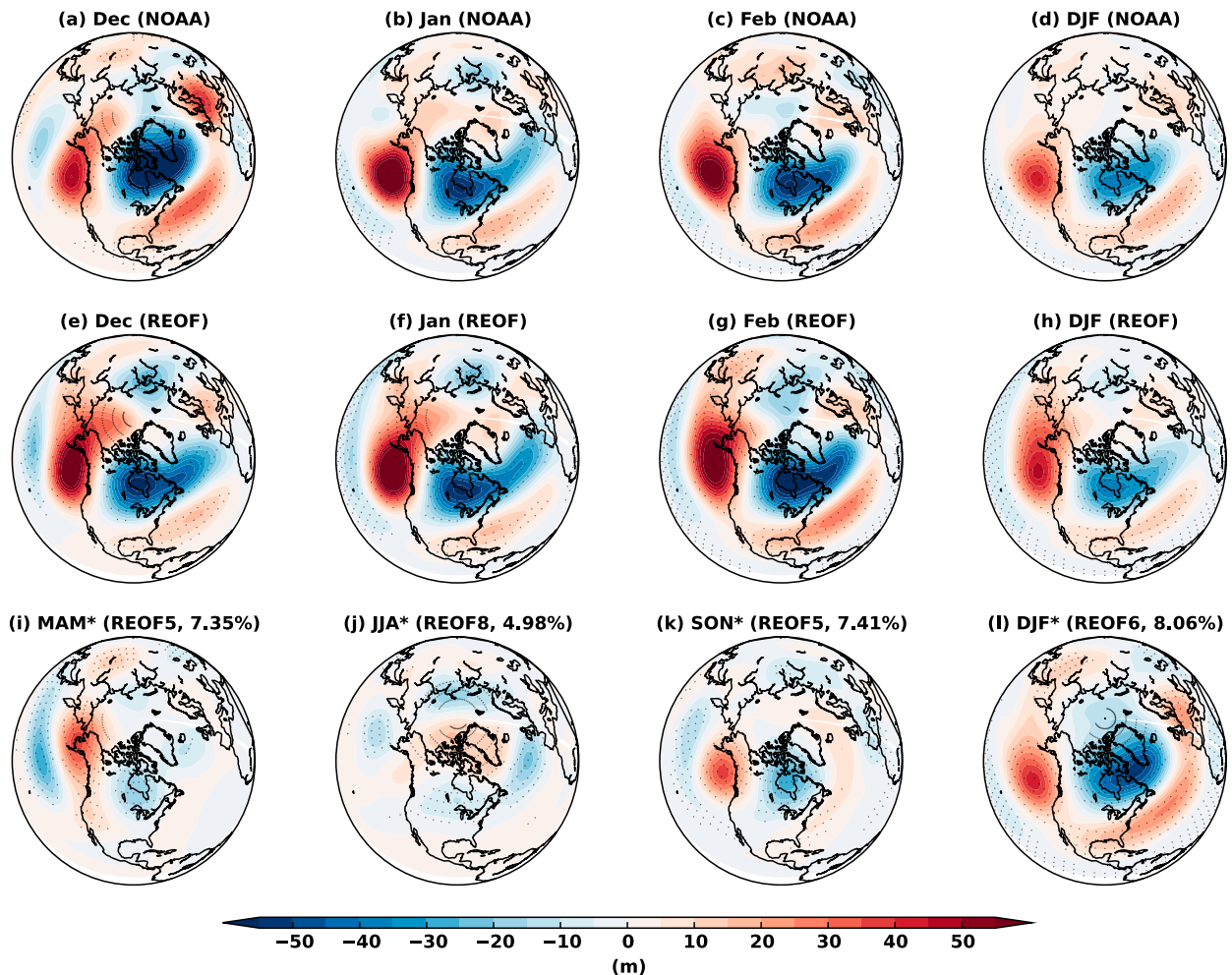
FIG. 1. The 500-mb geopotential height (Z500) anomalies regressed onto NOAA's TNH index for (a) December, (b) January, (c) February, and (d) the DJF average. (e)–(h) As in (a)–(d), but for our TNH index. (i)–(l) Regressed Z500 anomalies onto PCs derived from rotated EOF analysis separately for the different seasons. The numbers in the titles of (i)–(l) are the explained variance associated with each rotated EOF mode. The stippling indicates that the regression values are statistically significant (i.e., have p values less than 0.05).

Livezey 1987; Panagiotopoulos et al. 2002; Franzke and Feldstein 2005; Peng and Kumar 2005). The TNH circulation anomalies are suggested to produce anomalous surface temperatures and precipitation throughout the North American continents, subtropical North Pacific, and North Atlantic (for a comprehensive description, see http://www.cpc.ncep.noaa.gov/data/teledoc/tnh.shtml). Correlation-based analyses were first used to identify the TNH mode (e.g., Mo 1985; Mo and Livezey 1986), but these methods can suffer from difficulties in separating the TNH mode from other atmospheric circulation modes, especially when they co-occur. To avoid the possible mixture of different modes, a rotated empirical orthogonal function (REOF) analysis was also used to better distinguish the TNH mode from others (e.g., Mo and Livezey 1986; Barnston and Livezey 1987). The TNH mode was identified in Barnston and Livezey

(1987) as the fourth mode in January (explaining 9.8% of the total variance), the sixth mode in February (explaining 7.4% of the total variance), the ninth mode in November (explaining 4.9% of the total variance), and the ninth mode in December (explaining 6.3% of the total variance). These studies indicate that it is reasonable to identify the TNH pattern using the REOF method despite the fact that the pattern appears as a higher mode and explains less than 10% of the total variance.

In the present study, we applied the same REOF method of Barnston and Livezey (1987) to monthly 700-mb geopotential height (Z700) anomalies in the NH (20°–90°N) to identify the TNH pattern. The TNH pattern was identified as the ninth REOF mode, explaining 4.96% of the total variance, and its corresponding principal component was used as the TNH index in our study. We did not find a strong trend in the TNH index
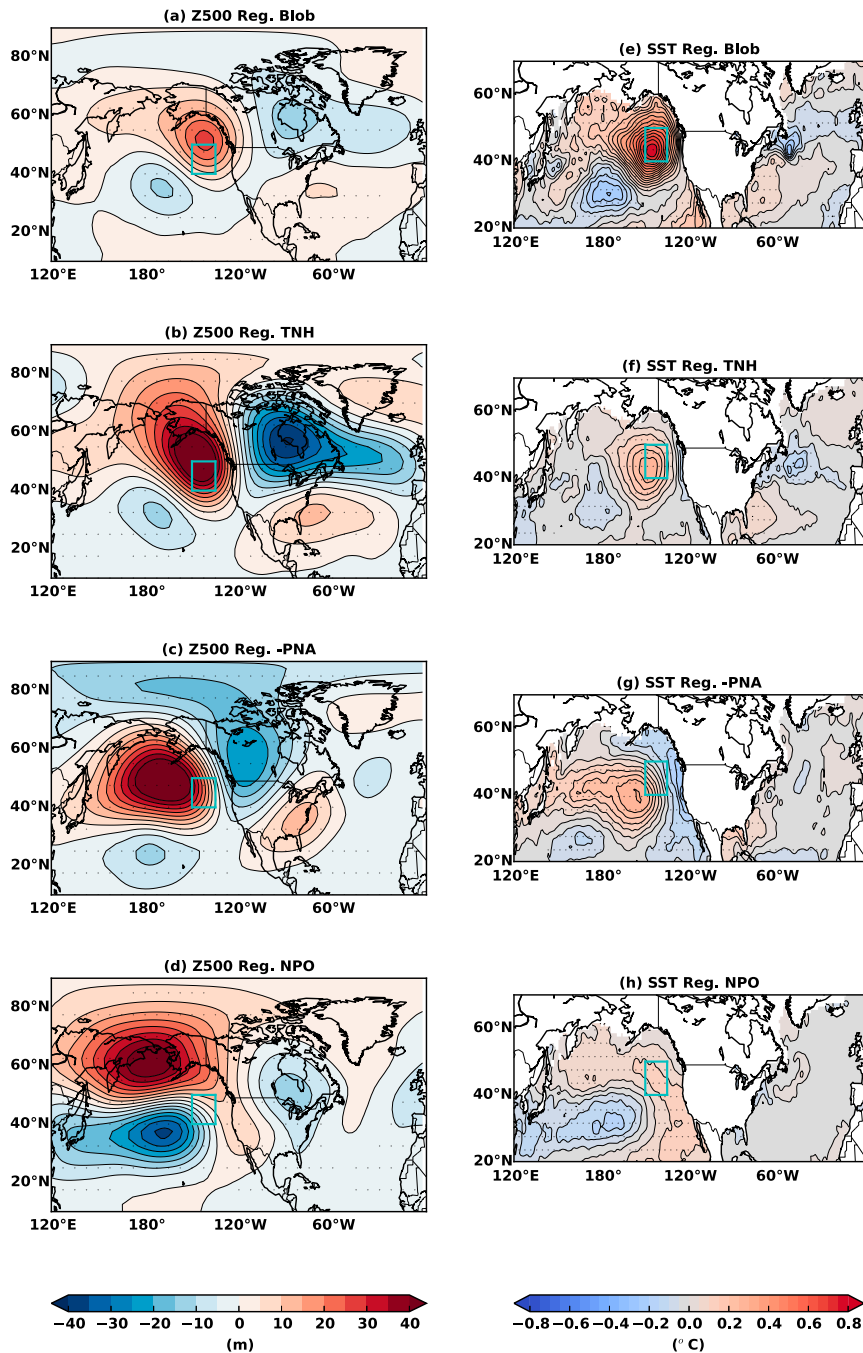
FIG. 2. Regression maps of 500-mb geopotential height (Z500) anomalies onto the (a) Pacific blob index, (b) TNH index, (c) negative PNA index, and (d) NPO index. Regression maps of SST anomalies onto the (e) Pacific blob index, (f) TNH index, (g) negative PNA index, and (h) NPO index. Contour intervals are 5 m in (a)–(d) and 0.05°C in (e)–(h). The light blue boxes delineate the Pacific blob region (40°–50°N, 150°–135°W) defined in Bond et al. (2015). The stippling indicates that the regression values are statistically significant (i.e., have *p* values less than 0.05).

and obtained similar results when applying the REOF analysis to the nondetrended Z700 fields. Our calculation is applied to all the data rather than just the NH winter months used in previous studies. To ensure our TNH calculation is correct, we first compared our TNH index to the NH winter [December–February (DJF)] values of the TNH index provided by NOAA's Climate Prediction Center. We found the correlation coefficients
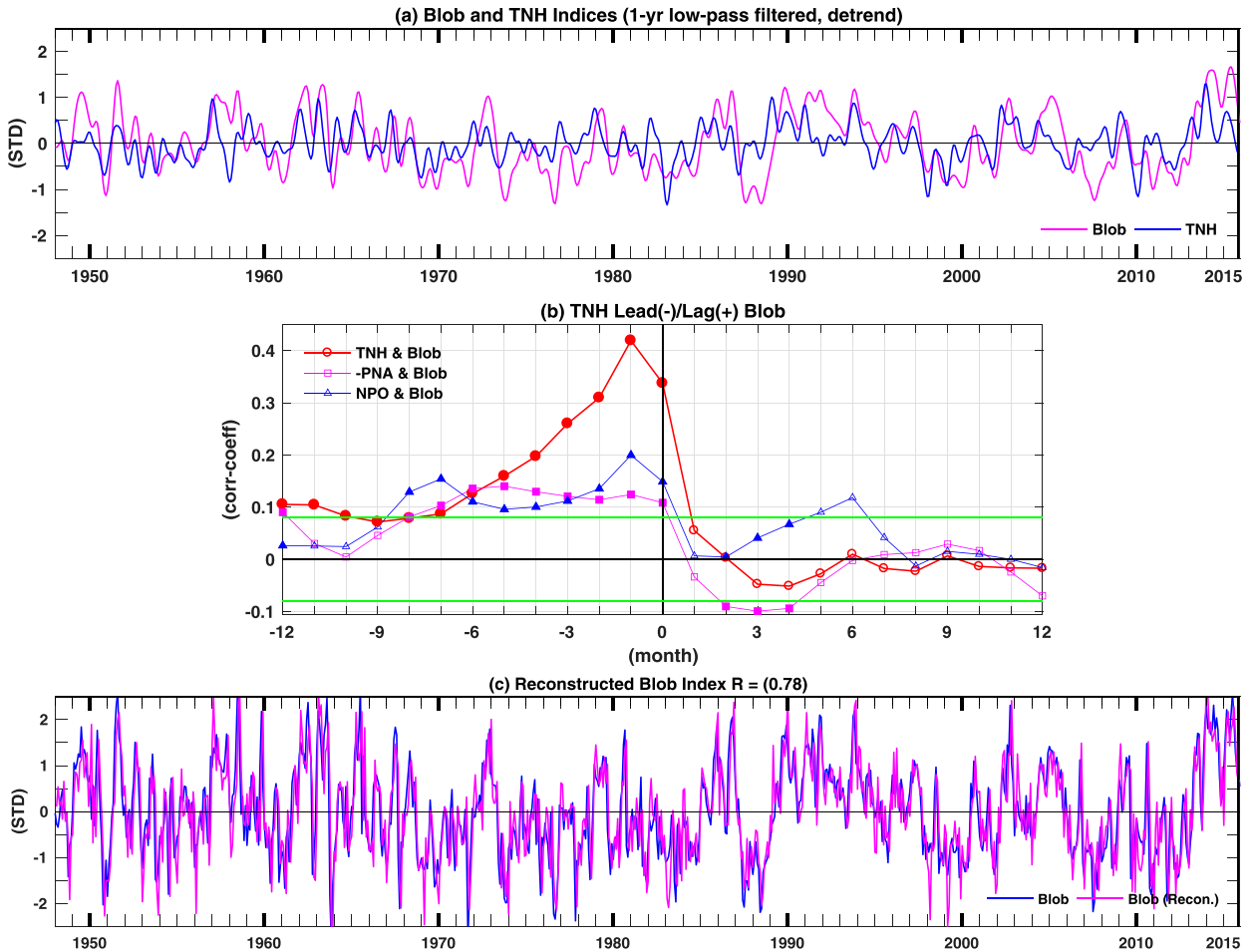
FIG. 3. (a) Temporal evolution of the Pacific blob and TNH indices during the period 1948–2015. (b) The lead–lagged relationships between the TNH (−PNA and NPO) and Pacific blob indices. The solid (open) marks denote correlation coefficients that have *p* values smaller (larger) than 0.05. The green lines in (b) delineate the 95% significance levels by considering the effective sample sizes determined based on Eq. (1). (c) The AR1 model-reconstructed Pacific blob index (pink) including the TNH forcing term as described in Eq. (2), and the original blob index (blue). Note that the lead–lagged correlation coefficients and reconstructed blob index are calculated using unfiltered time series.

between them to be high for all three winter months (i.e., 0.74 for December, 0.86 for January, 0.86 for February, and 0.82 for the DJF average). We then compared the wintertime 500-hPa geopotential height (Z500) anomalies regressed onto NOAA's TNH index (Figs. 1a–d) and those regressed onto ours (Figs. 1e–h) and find their pattern correlations to be high (i.e., 0.73 for December, 0.91 for January, 0.87 for February, and 0.92 for DJF average) over the study region (20°–80°N, 120°E–20°W). Lead–lagged regression analyses of Z700, Z500, and 200-hPa geopotential height (Z200) anomalies with these two indices also reveal similar temporal evolutions (not shown).

We also examined the seasonality in the TNH pattern by repeating the REOF analysis to each of the four seasons (Figs. 1i–l). The TNH mode appears as the fifth mode in spring (explaining 7.35% of the total variance), the eighth mode in summer (explaining 4.98% of the total variance), the fifth mode in autumn (explaining 7.41% of the total variance), and the sixth mode in winter (explaining 8.06% of the total variance). This analysis confirms that the TNH pattern exists throughout the year and that it is strongest during winter/spring and weakest during summer.

To determine statistical significance in our correlation analysis, the effective number of degrees of freedom $\tilde{N}$ is calculated following Bretherton et al. (1999):

$$\tilde{N} = N(1 - r_x r_y)/(1 - r_x r_y), \qquad (1)$$

where N is the sample size of the original time series and r_x and r_y are the lag-1 autocorrelations of the time series
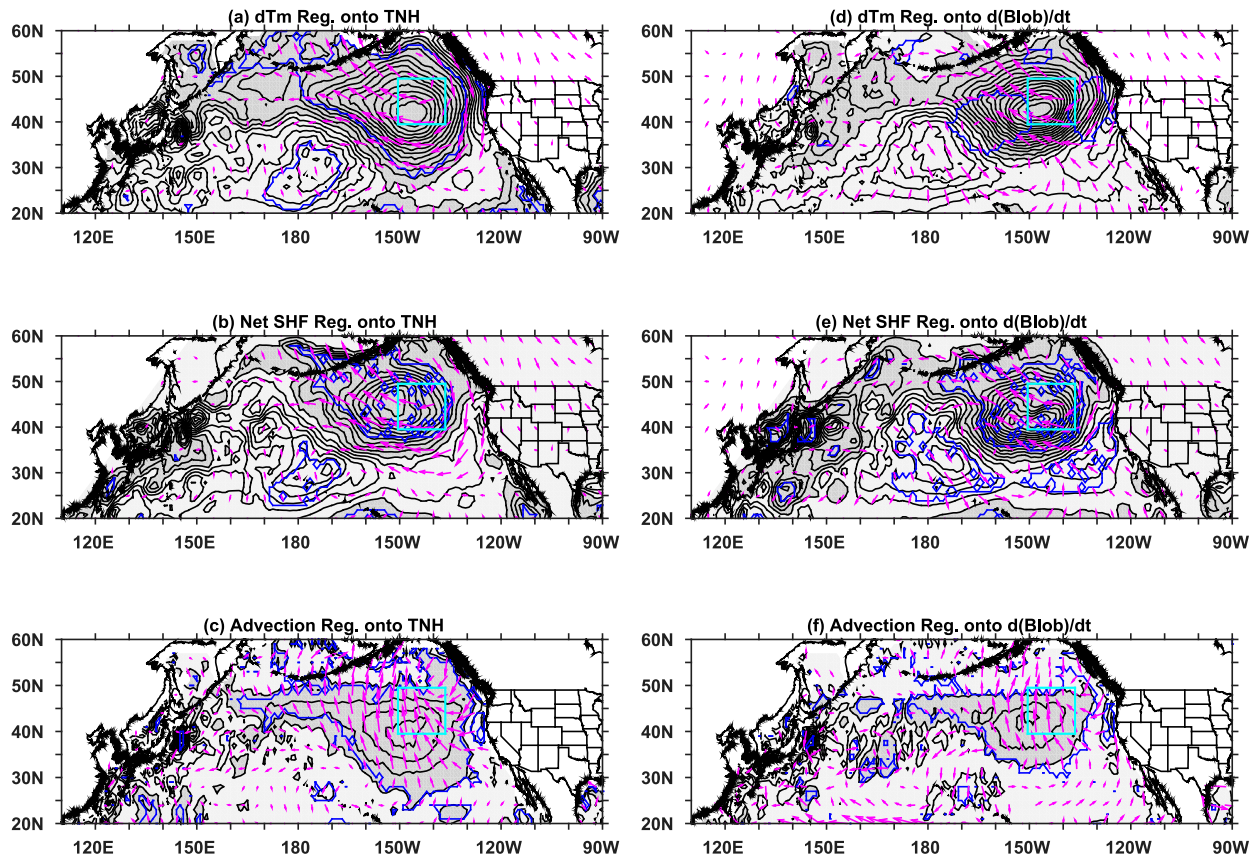
FIG. 4. (a) The mixed layer temperature tendency (dT_m/dt), (b) the net SHFs (positive into the ocean), and (c) the horizontal ocean advection regressed onto the TNH index. (d)–(f) As in (a)–(c), but values are regressed onto the time tendency of the Pacific blob index (i.e., dBlob$/dt$). Contour intervals are 0.01°C month^{-1}. The shaded regions represent positive values while the unshaded areas represent negative values. The pink arrows in (a),(b),(d),(e) are the regressed 1000-mb wind anomalies while those in (c),(f) are the regressed 5-m ocean current anomalies. The light blue boxes delineate the Pacific blob region (40°–50°N, 150°–135°W) defined in Bond et al. (2015). The blue contour lines indicate the 95% significance level.

x and y that are being correlated. If correlation analysis is applied to filtered time series, the r_x and r_y are replaced by the lag-1 autocorrelations of the filtered time series x and y.

3. The relationship between the TNH pattern and the Pacific warm blob

To investigate which large-scale atmospheric circulation pattern is closely associated with the Pacific blob, we regressed the Z500 anomalies onto the Pacific blob index. This regression pattern (Fig. 2a) closely resembles the Z500 pattern regressed onto the TNH index (Fig. 2b), both of which are characterized by a wave train structure with anomaly centers emanating from the subtropical Pacific and passing through the anomalous ridge region in the NE Pacific and a meridional dipole structure extending zonally from North American continents to the North Atlantic. In contrast, the PNA and NPO

patterns (Figs. 2e,g) show geographical features differing from the blob-regressed pattern. In the North Pacific sector, the wave train structure in the blob-regressed pattern is distinct from the meridional dipole structures in the PNA or NPO patterns. In the North Atlantic sector, the zonally elongated structure is absent in the PNA pattern and is almost orthogonal to the dipolar structure of the NPO pattern. To further verify the spatial similarities/differences, pattern correlation coefficients were calculated between the regressed Z500 pattern onto the Pacific blob index and those regressed onto the TNH, PNA, or NPO indices over the North Pacific–Atlantic sector (20°–80°N, 120°E–20°W). The pattern correlation coefficient for the TNH pattern (0.83) is much larger than those for the PNA (0.15) or NPO (0.48) patterns. Comparing the blob- and TNH-regressed SST anomaly patterns (Figs. 2e,f), we also found both to be associated with large SST anomalies near the Pacific blob region that resemble
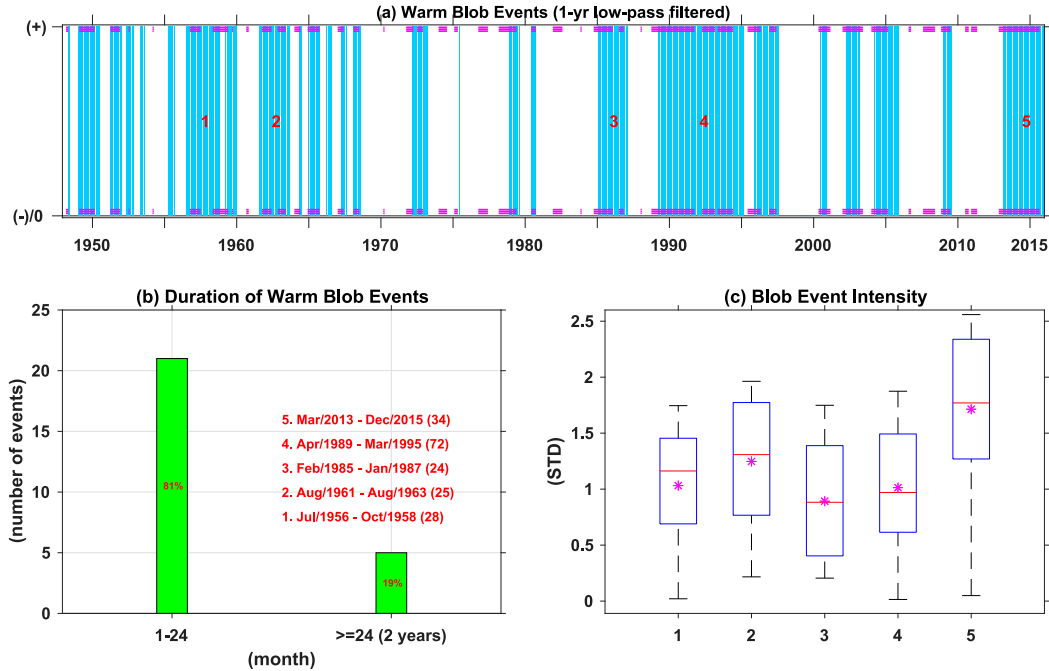
FIG. 5. (a) Phase analysis of the Pacific blob and the TNH indices. The light blue (white) shadings indicate the positive (negative) phase of the blob index. The pink bars indicate the positive phase of the TNH index, and the red numbers represent the five prolonged Pacific warm blob events. (b) Duration analysis of the positive values of the Pacific blob index. In (b), the values on the *y* axis represent the number of events, the numbers inside the bars indicate the percentage of these Pacific warm blob events, the exact starting and ending dates of events having duration times larger than 2 years are listed above the right bar, and the values in the parentheses represent the exact duration in months. (c) Box-and-whisker plot for the SST anomalies for each prolonged Pacific blob event. The top and bottom of the blue box denote the 75th and 25th percentiles of the blob SST samples, the red line represents the median of the blob SST anomalies, the pink star is the mean of the blob SST anomalies, and the top and bottom of the whisker dashed lines are the highest and lowest blob SST anomalies in each event. The indices used here were 1-yr low-pass filtered.

the GOA warming pattern observed during the 2013–15 blob event (e.g., Amaya et al. 2016; Di Lorenzo and Mantua 2016), but different from the PNA- and NPO-regressed SST anomalies (Figs. 2g,h). It is obvious that the TNH pattern, not the PNA or NPO pattern, is the large-scale atmospheric circulation pattern closely associated with the Pacific blob. It is noted that there are some differences in magnitude between the TNH- and blob-regressed SST patterns, which reflects the fact that other processes may affect the SST variability in the Pacific blob region.

We then compared the evolutions of the TNH and the Pacific blob indices in Fig. 3a. The figure shows that the warm phase of the Pacific blob largely coincides with the positive phase of the TNH pattern. We applied a 1-yr low-pass filter to smooth the indices in Fig. 3a to better illustrate their evolution and to remove high-frequency fluctuations. The lead–lagged correlation analysis between the original unfiltered indices in Fig. 3b shows that the maximum correlation coefficient (0.42) occurs when the TNH index leads the Pacific blob index by one

month. This relation indicates that it is the TNH pattern that forces the Pacific blob rather than the other way around. We also calculated the lead–lagged correlation coefficients of the PNA and NPO indices with the Pacific blob index (Fig. 3b) and found them to be much smaller than the correlation coefficients between the TNH and Pacific blob indices.

The close association between the TNH pattern and the Pacific blob can be further verified by a first-order autoregressive (AR1) model, a widely used tool for quantifying the ocean response to forcing from the atmosphere in the North Pacific (e.g., Newman et al. 2003; Schneider and Cornuelle 2005; Johnstone and Mantua 2014; Di Lorenzo and Mantua 2016). Following these previous studies, we construct a Pacific blob index according to the AR1 model formulation as follows:

$$\mathrm{Blob}_{t+1} = \alpha \mathrm{TNH}_t + \beta \mathrm{Blob}_t + \varepsilon_t, \tag{2}$$

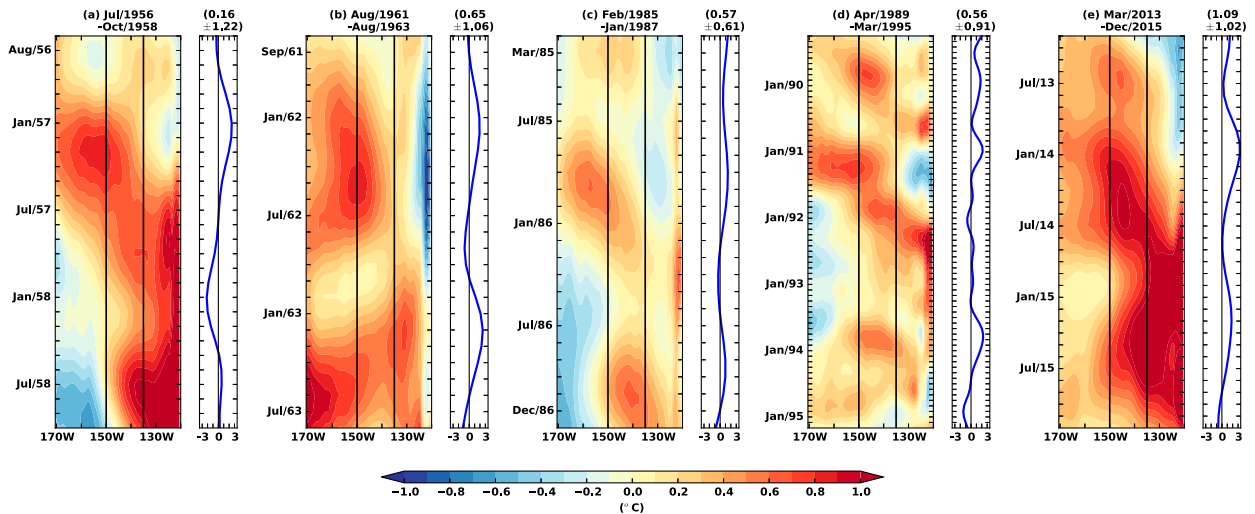where the TNH and Blob terms on the right-hand side denote the TNH forcing and the blob SST damping, and

FIG. 6. Hovmöller diagrams for the SST anomalies averaged between 40° and 50°N after application of a 1-yr low-pass filter. The vertical black lines represent the longitudes of the Pacific blob boundaries (i.e., 150° and 135°W). The 1-yr low-pass-filtered TNH indices during these events are shown by the blue lines next to the Hovmöller diagrams. The first value in the parentheses indicates the mean of the TNH index over each event, while the value after the "±" sign is the standard deviation over each event.

ε_t represents uncorrelated Gaussian-type random noise. The coefficient α (0.42) is obtained by regressing the Pacific blob index (i.e., Blob_{t+1}) against the TNH index with 1-month lag time (i.e., TNH_t). The coefficient β (0.77) is calculated by regressing the Pacific blob index, after removing the TNH information (i.e., $\text{Blob}_{t+1} - \alpha\text{TNH}_t$), against the original Pacific blob index with 1-month lag time (i.e., Blob_t). As shown in Fig. 3c, the reconstructed blob index matches the original blob index reasonably well with a high correlation coefficient of 0.78. This result indicates that about 61% of the Pacific blob variability can be accounted for by the TNH forcing and adds additional support to our suggestion that the TNH pattern can force the Pacific blob.

To uncover the mechanisms by which the TNH pattern forces the Pacific blob, we performed an ocean mixed layer heat budget analysis (similar to that performed in Bond et al. 2015) over the North Pacific domain (see Fig. 4). We first calculated the monthly values of the mixed layer temperature tendency (dT_m/dt), net surface heat fluxes (SHF, positive downward), and horizontal ocean advection, and then regressed them onto the TNH index and the time tendency of the blob index (i.e., $d\text{Blob}/dt$). When determining the ocean advection, we first integrated the ocean current velocity and potential temperature from ocean surface to the bottom of the mixed layer, and then calculated the horizontal temperature gradient and its dot product with the integrated velocities. The regressed dT_m/dt patterns are characterized by the GOA warming pattern with a center in the Pacific blob region and a cooling band

along the U.S. West Coast that extends toward the subtropical Pacific (Figs. 4a,d). These regions of warming and cooling tendencies largely coincide with positive and negative SHF anomalies (Figs. 4b,e). The positive SHF anomalies in the Pacific blob region are associated with near-surface wind anomalies regressed onto the TNH index and $d\text{Blob}/dt$ (pink arrows in Figs. 4b,e), both of which are dominated by clockwise near-surface wind anomalies relating to the anomalous ridge. The southern and eastern branches of the clockwise wind anomalies weaken the prevailing westerlies, decrease the SHF, and produce a warming tendency. Further examination on the TNH-regressed horizontal ocean advection anomalies (Fig. 4c) show that warm anomalies, induced by the anomalous easterly winds, also contribute to the warming tendency (0.069°C month^{-1}) in the Pacific blob region, but are only about one-third as large as the SHF-induced warming (0.21°C month^{-1}). We also investigated the vertical heat exchange at the bottom of the mixed layer (i.e., entrainment), estimated by the wind stress curl and found slightly negative anomalies induced in the Pacific blob region (not shown). These results are consistent with those in Bond et al. (2015) and indicate that the TNH-induced entrainment anomalies are relatively weak. This mixed layer heat budget analysis suggests that the TNH pattern forces the Pacific blob primarily through anomalies in SHF and secondarily through anomalies in wind-induced ocean advection.

We noticed from Fig. 3a that, when the 2013–15 Pacific blob warming occurs, the TNH pattern has the tendency to stay in its positive phase for a similar period
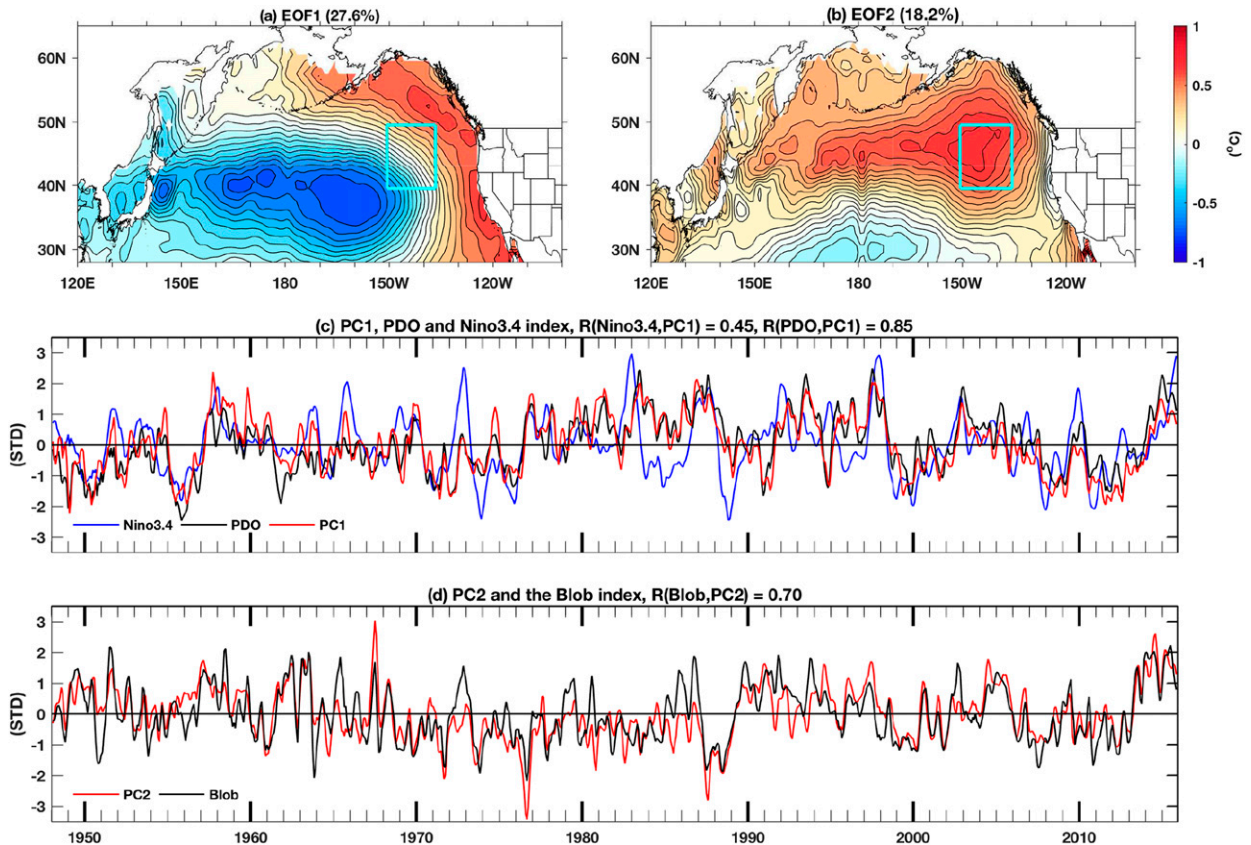
FIG. 7. (a),(b) The loading coefficient patterns for the first and second EOF modes of the North Pacific SST variability, where the units have been converted to °C using their corresponding eigenvalues. The light blue boxes in (a) and (b) delineate the Pacific blob region (40°–50°N, 150°–135°W) defined in Bond et al. (2015). Contour intervals are 0.1°C. (c) The evolution of the principal component of the first EOF mode (i.e., PC1), the PDO index, and the Niño-3.4 index. (d) The evolution of the principal component of the second EOF mode (i.e., PC2) and the Pacific blob index. Time series in (c) and (d) are averaged using a 3-month window.

of time. To investigate this phase consistency between the TNH and Pacific blob indices, we performed a phase analysis in Fig. 5a to explicitly identify the periods when the Pacific blob index has positive values (blue shading) and the periods when the TNH index has positive values (pink bars) during 1948–2015. The figure indicates that, for a majority of the periods when the Pacific blob index stays in its positive phase, the TNH index also stays in its positive phase. We pay particular attention to the periods when Pacific blob warming lasts exceptionally long (similar to the 2013–15 event), and define a prolonged Pacific blob event as one having warming for at least 24 months. Five such prolonged events (including the 2013–15 event) during 1948–2015 can be identified, and they account for 19% of the total number of the positive-blob periods (Fig. 5b). These five prolonged blob events occurred during July 1956–October 1958, August 1961–August 1964, February 1985–January 1987, April 1989–March 1995, and March 2013–December 2015. After marking all these events in Fig. 5a (the red numbers), we

found that the TNH index was locked into its positive phase through a major portion of each event. These results indicate that locking the TNH pattern into its positive phase for an extended period plays a critical role in forcing prolonged Pacific blob events. We also examined the blob intensity by showing in Fig. 5c the mean, maximum, and minimum values of the blob index during these prolonged blob events. All prolonged events we selected have strong intensity (means >0.8 and maxima >1.5 standard deviations), with the 2013–15 event being the strongest.

To better illuminate the SST evolutions and the TNH phase-locking feature during the five prolonged blob events, we show in Fig. 6 Hovmöller diagrams for the SST anomalies averaged between 40° and 50°N. The values of the TNH index during these events are shown next to the Hovmöller diagram. The figure clearly shows that the TNH index stays mostly in its positive phase during these events, which is also shown by the positive mean TNH values. The 2013–15 event has the highest
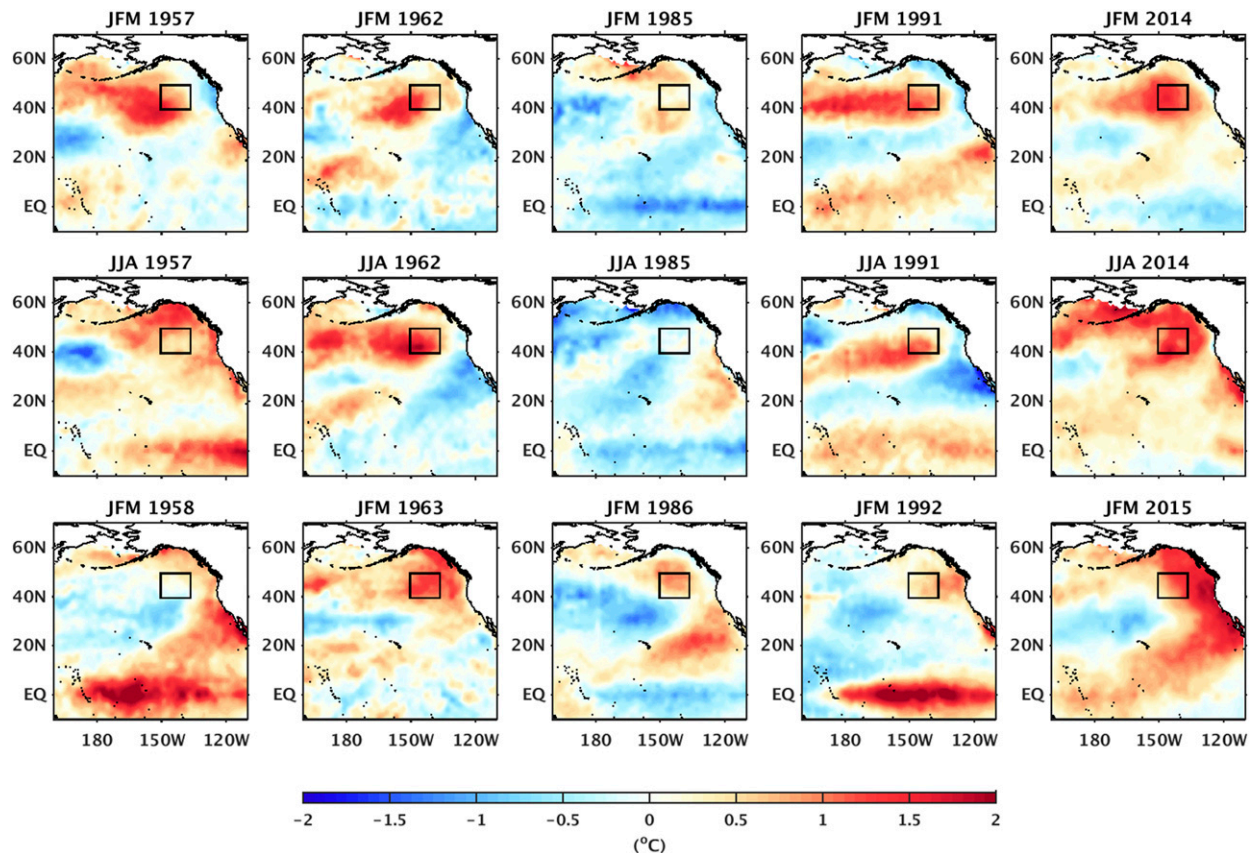
FIG. 8. The SST anomalies averaged in winter (JFM) and summer (JJA) seasons for the five prolonged blob events. The black boxes delineate the Pacific blob region (40°–50°N, 150°–135°W) defined in Bond et al. (2015).

mean TNH value (1.09), followed by the 1961–63 (0.65), the 1985–87 (0.57), the 1989–95 (0.56), and the 1956–58 (0.16) events. These positive TNH means correspond well to the positive mean values of the blob index during these events, which provides additional support for a close association between the TNH phase-locking and prolonged blob events.

4. Relationships of the Pacific warm blob to PDO and ENSO

The PDO and ENSO can also produce SST anomalies near the Pacific blob region (Mantua et al. 1997; Alexander et al. 2002; Newman et al. 2003). To examine the possible relationships of the Pacific blob to PDO and ENSO, we performed a covariance-based EOF analysis on SST anomalies in the North Pacific region (17°–60°N, 120°–100°W). The first EOF mode (EOF1; explains 27.6% of total variance; Fig. 7a) resembles the PDO SST pattern, characterized by a cooling in the central North Pacific and a band of warming along the North American coasts resembling the ARC SST pattern. The principal

component of EOF1 mode (PC1) follows closely with the PDO index during the analysis period (Fig. 7c) with a high correlation coefficient between them (0.85), in contrast to the low correlation coefficient between PC1 and the Pacific blob index (0.07). The EOF2 mode (explains 18.2% of total variance; Fig. 7b) is characterized by SST anomalies in the NE Pacific that resembles the GOA pattern with its anomaly center appearing inside the Pacific blob box. The PC2 is found evolving closely with the Pacific blob index (Fig. 7d) with a correlation coefficient of 0.70. This EOF analysis clearly shows that the Pacific blob is not associated with the PDO and is a separate dynamical entity.

One important signature shown in EOF1 mode is the band of warming off North American coasts that is similar to the ARC warming pattern observed in the 2013–15 Pacific blob event. As mentioned, SST anomalies during that blob event involved a shift from a GOA warming pattern to an ARC warming pattern (Amaya et al. 2016; Di Lorenzo et al. 2016; Di Lorenzo and Mantua 2016). Is such a shift a necessary component of Pacific blob generation? We analyze the evolution of the SST anomalies in the five prolonged blob events (Fig. 8)
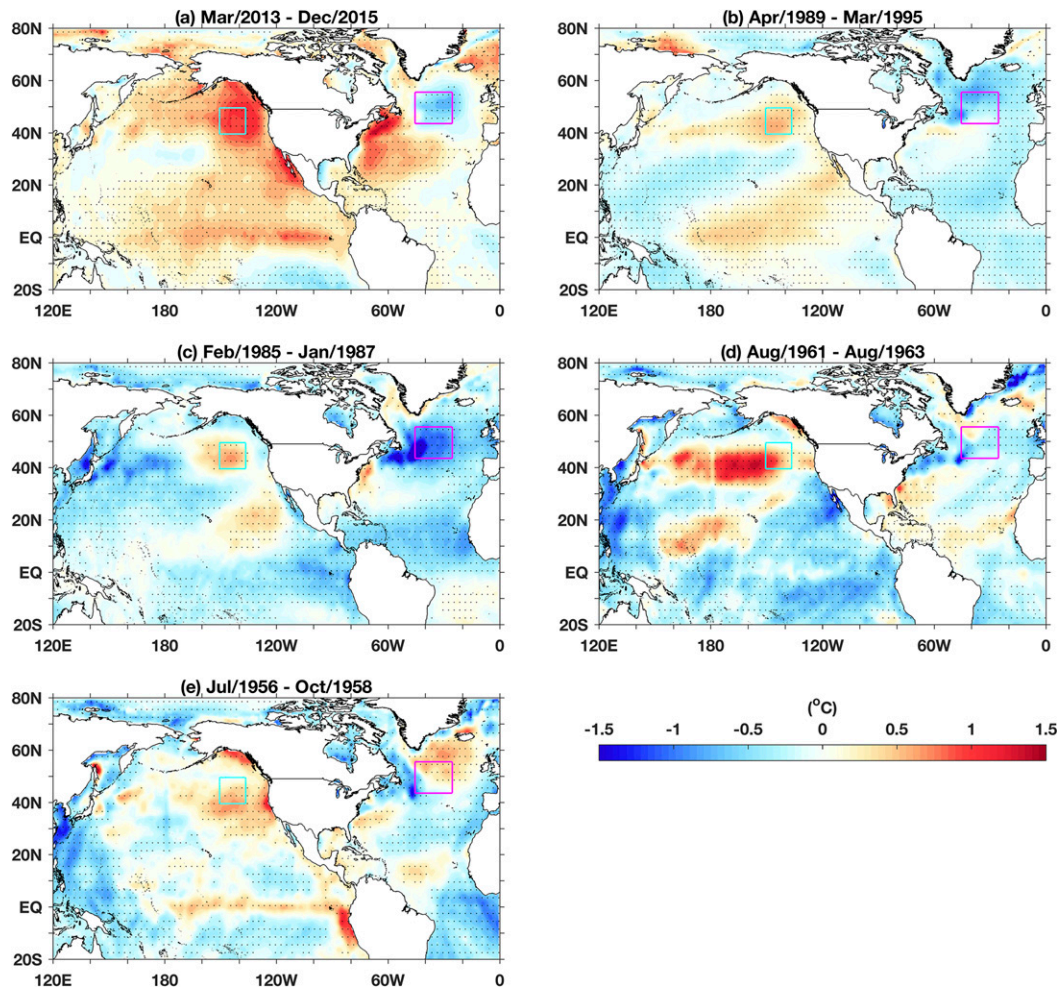
FIG. 9. Composited SST anomalies for the five prolonged blob events: (a) March 2013–December 2015, (b) April 1989–March 1995, (c) February 1985–January 1987, (d) August 1961–August 1963, and (e) July 1956–October 1958. The light blue boxes delineate the blob region (40°–50°N, 150°–135°W) defined in Bond et al. (2015), whereas the pink boxes depict the Atlantic cold region (44°–56°N, 45°–25°W). The stippling indicates that the composite anomalies are statistically significant at the 95% level according to the Student's two-tailed t test.

and find that only two of them (the 1957–58 and 2014–15 events) exhibit a shift from the GOA to ARC warming pattern. It is noted that these two blob events were accompanied by El Niño conditions in the tropics. Therefore, El Niño possibly triggers the ARC-to-GOA shift in the prolonged blob events, as has been suggested by several recent studies (e.g., Amaya et al. 2016; Di Lorenzo et al. 2016; Di Lorenzo and Mantua 2016), but is not a necessary mechanism for Pacific blob generation.

5. The relationship between the TNH pattern and the Atlantic cold blob

An interesting feature of the TNH pattern is that its anomaly structures crossing both the North Pacific and North Atlantic (see Fig. 2b). This implies that when the TNH pattern stays in its positive phase for an extended period of time to force a Pacific warm blob event, it may also force SST variability in the North Atlantic. This possibility is revealed by the TNH-regressed SST anomaly pattern (Fig. 2f), where statistically significant negative SST anomalies are found in the North Atlantic. The location of the cold anomalies is close to where the Atlantic cold blob was observed during 2014–15 (Henson 2016), as shown in the SST anomalies averaged in this event (Fig. 9a). Such Atlantic cold blobs are also observed in the SST anomalies averaged in the other four prolonged Pacific warm blob events (Figs. 9b–e), although the intensity of the Atlantic blob is weaker in the 1956–58 event. The co-occurrence of Pacific warm blob and Atlantic cold blob in these five events reveals
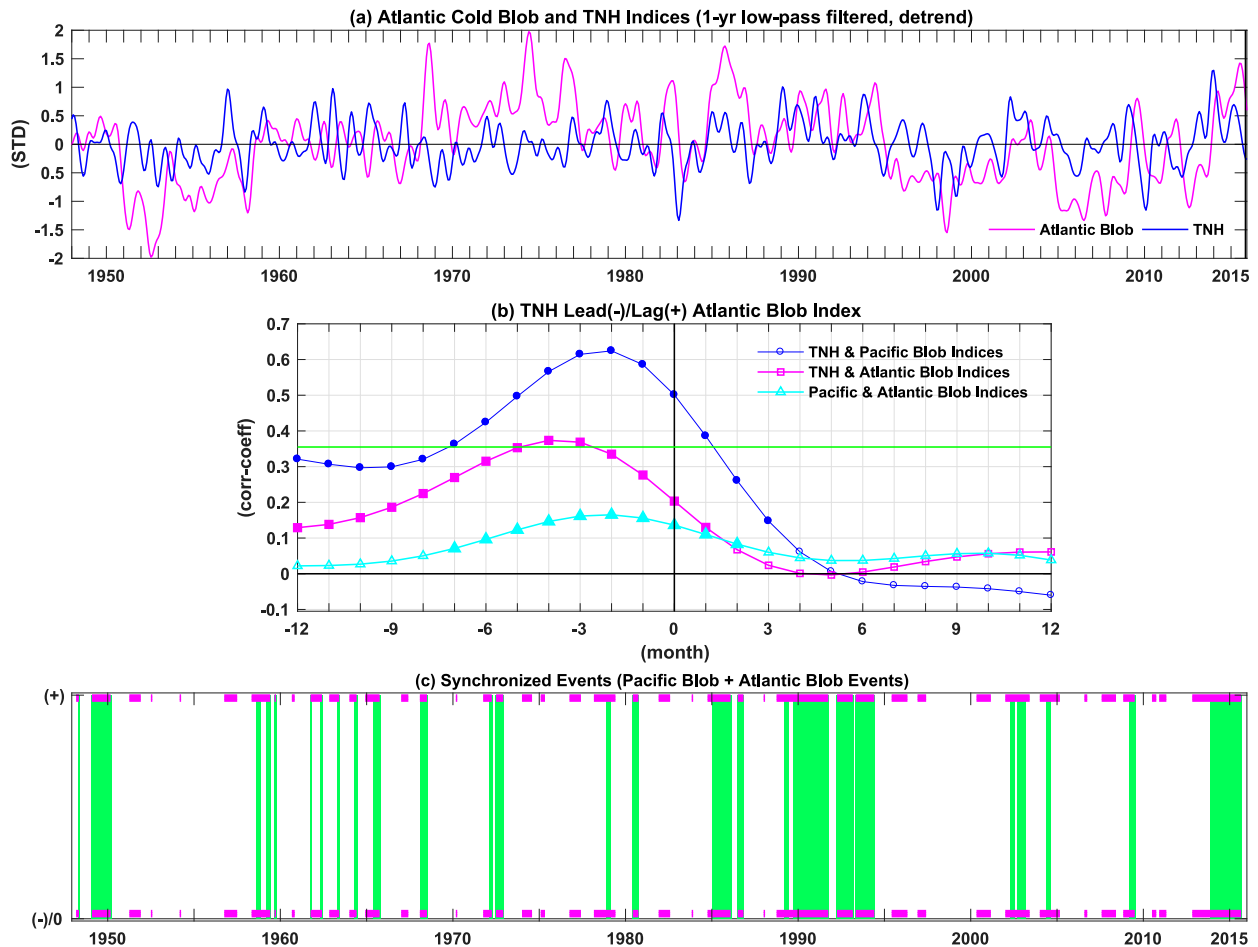
FIG. 10. (a) Temporal evolution of the Atlantic cold and TNH indices during the period 1948–2015. (b) The lead–lagged relationships between the TNH, Atlantic blob, and Pacific blob indices. The solid (open) marks denote correlation coefficients that have p values smaller (larger) than 0.05. Note that the lead–lagged correlation coefficients are calculated using filtered time series. The green lines in (b) delineate the 95% significance levels by considering the effective sample sizes determined based on Eq. (1). (c) Phase analysis for the occurrences of the Pacific warm blob and Atlantic cold events. The light green shading indicates the positive phases of both the Pacific blob and Atlantic cold indices. The pink bars indicate the positive phase of the TNH index. The indices used for the phase analysis were 1-yr low-pass filtered.

that the TNH pattern may serve as a conducting mechanism to connect some of them.

Figure 10a exhibits that the TNH and the Atlantic cold blob indices have a tendency to follow each other during the analysis period. The lead–lag correlation analysis shows that the 1-yr low-pass-filtered TNH index has the largest correlation coefficient (0.37) with the filtered Atlantic blob index when the former leads the latter by 4 months (Fig. 10b), which is longer than the 2-month lead time found between the filtered TNH and Pacific blob indices. A 2-month lead time is also found in the lead–lag correlation analysis between filtered Pacific blob and the Atlantic blob indices. These lead–lagged relations likely reflect the fact that the mean mixed layer is deeper in the Atlantic blob region (118.7 m) than in the Pacific blob region (48.1 m),

indicating the TNH pattern requires more time to induce Atlantic cold blob than Pacific warm blob. Figure 10b also reveals that the correlation coefficients between the TNH and the Pacific blob indices are higher than those between the TNH and the Atlantic blob indices, which implies that the TNH pattern accounts for more SST variability in the Pacific blob region than that in the Atlantic blob region. Other major forcing mechanisms also exist for the Atlantic cold blobs, such as those associated with the NAO, the AMOC, and the Greenland ice sheet melting (Delworth et al. 2016; Yeager et al. 2016; Rahmstorf et al. 2015; Robson et al. 2016; Duchez et al. 2016; Schmittner et al. 2016). This study indicates that TNH forcing is an additional, rather than an exclusive, explanation for the generation of the Atlantic blob.

To further examine the connection between Pacific and Atlantic blobs, we show in Fig. 10c the periods when positive values of the Pacific blob index coincide with positive values of the Atlantic blob index (green shading). Also shown in the figure are the periods when the TNH pattern stays in its positive phase (pink bars). The Pacific warm blob events have co-occurred with Atlantic cold blob events several times during the analysis period, mostly when the TNH pattern persistently stayed in its positive phase. Among them, 1985–87, the early 1990s, and 2013–15 are the three longest periods when the Pacific and Atlantic blobs are synchronized. The evidence suggests that the TNH pattern is able to connect some of the prolonged Pacific warm blobs and Atlantic cold blobs. A mixed layer heat budget analysis over the North Atlantic (Fig. 11) confirms that the TNH pattern forces the Atlantic blob cooling mainly via anomalies in SHF ($-0.18°$C month^{-1}) and secondarily via anomalies in horizontal ocean advection ($-0.026°$C month^{-1}).

To assess the importance of the TNH pattern in establishing the climate connectivity between the North Pacific and North Atlantic, we perform a maximum covariance analysis (MCA; Wallace et al. 1992) to Z500 and SST anomalies over these two oceans during the analysis period. We calculate these MCA modes by assuming the Z500 field leads the SST field by one month as shown in Fig. 3b. The first MCA (MCA1) mode (explains 42% of the squared covariance; Figs. 12a,b) is characterized by a Z500 anomaly pattern similar to the PNA pattern (Fig. 2c) and an SST anomaly pattern similar to the ARC warming pattern (Fig. 7a). The correlation coefficients between the MCA1 PCs and the PNA and PDO (Niño-3.4) indices are 0.72 and 0.80 (0.44), respectively. The MCA1 mode is related to the PDO or ENSO and their associated atmospheric circulation patterns. This mode has large anomalies over the Pacific sector but small anomalies over the Atlantic sector and contributes little to the climate connectivity between the North Pacific and North Atlantic. In contrast, the second MCA (MCA2) mode (explains 22% of the squared covariance; Figs. 12c,d) is characterized by Z500 and SST anomalies crossing both the North Pacific and North Atlantic. Its Z500 pattern closely resembles the TNH pattern with a pattern correlation coefficient of 0.78 and a Z500 PC correlation coefficient of 0.66 with the TNH index. The SST anomaly pattern of MCA2 mode is characterized by a warming center in the Pacific blob region and a cooling center in the Atlantic blob region (Fig. 12d). Its SST PC has high correlation coefficients with both the Pacific blob index (0.64) and the Atlantic blob index (0.76). This MCA mode suggests 1) that the connection between the Pacific blob and
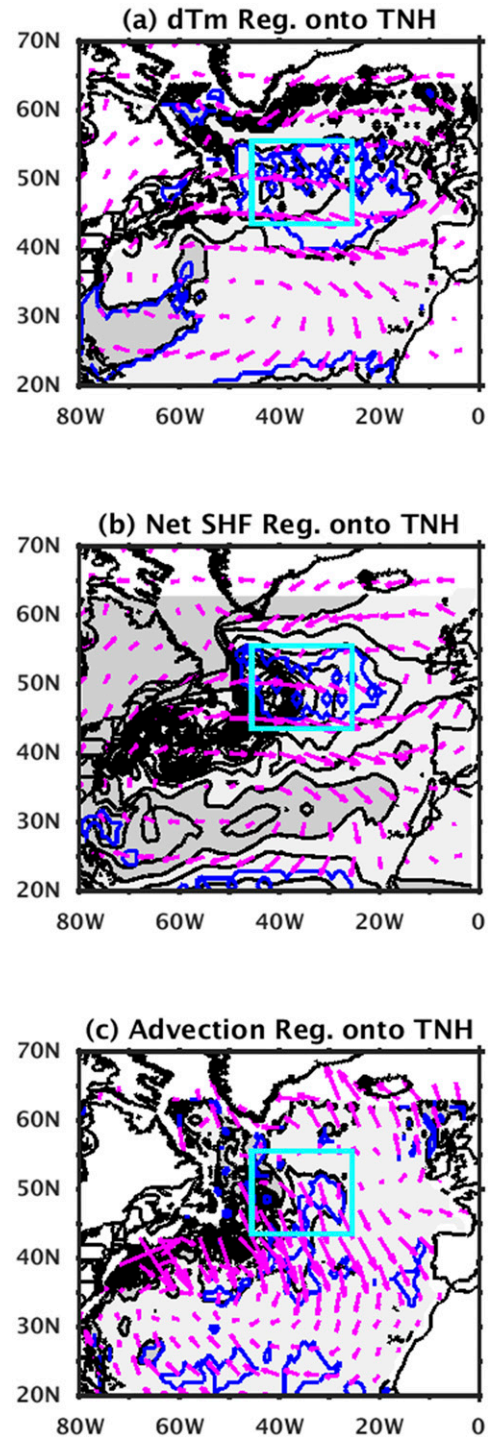

FIG. 11. (a) The mixed layer temperature tendency (dT_m/dt), (b) the net SHFs (positive into the ocean), and (c) the horizontal ocean advection regressed onto the TNH index. Contour intervals are 0.01°C month^{-1}. The shaded regions represent positive values while the unshaded areas represent negative values. The pink arrows in (a) and (b) are the regressed 1000-mb winds anomalies while those in (c) are the regressed 5-m ocean current anomalies. The light blue boxes depict the Atlantic cold region (44°–56°N, 45°–25°W). The blue contour lines indicate 95% significance level.
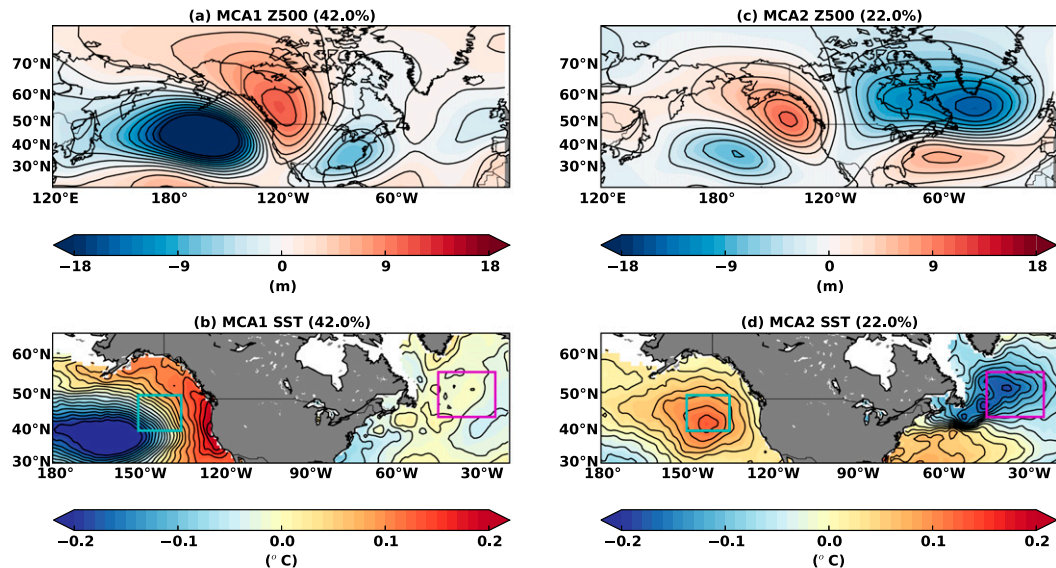
FIG. 12. The two leading modes of an MCA analysis of the combined Z500 (20°–90°N, 120°E–0°) and SST (30°–65°N, 180°–20°W) anomalies in the North Pacific–Atlantic Oceans with the Z500 field leading the SST field by one month. (a),(b) The Z500 and SST patterns associated with the first leading MCA mode. (c),(d) The patterns associated with the second leading mode. The number in the parentheses of each panel represents the percentage of squared covariance between Z500 and SST fields explained by the MCA mode. The light blue boxes delineate the Pacific blob region (40°–50°N, 150°–135°W) defined in Bond et al. (2015), whereas the pink boxes depict the Atlantic cold region (44°–56°N, 45°–25°W).

Atlantic blob is the second leading atmosphere–ocean coupled mode in the North Pacific–Atlantic sector and 2) that the TNH pattern is the key atmospheric circulation pattern to establish the climate connectivity between the two oceans.

6. Summary and discussion

This study argues that the TNH pattern is the principle atmospheric circulation pattern involved in the generation of the Pacific warm blob. Prolonged warm blob events occurred together with extended episodes of positive phases of this atmospheric circulation pattern. The TNH–blob relationship is verified by performing statistical analyses and case studies of the five prolonged Pacific warm blob events during the analysis period (1948–2015). This study also finds that the shift from a GOA warming pattern to an ARC warming pattern is not a necessary feature of Pacific blob generation. This shift occurs if an El Niño develops during a Pacific blob event, such as during the 2013–15 Pacific warm blob event. The core part of the Pacific warm blob is the GOA warming pattern, which is closely tied to the TNH forcing. EOF analysis demonstrated that the Pacific warm blob is not part of the PDO or ENSO and is a separate dynamical entity.

This study further shows that the cross-basin structure of the TNH pattern enables it to force SST variability in both the Pacific blob and Atlantic blob regions. As a result, some of the Pacific warm blob events occurred together with some of the Atlantic cold blob events. This connection between the Pacific warm blob and Atlantic cold blob appears as a leading covariability mode in the North Pacific–Atlantic sector. Three of the five prolonged Pacific warm blob events were accompanied by prolonged Atlantic cold blob events. It is important to note that the TNH contribution to the generation of the Pacific warm blob is larger than its contribution to the generation of the Atlantic cold blob. Factors other than the TNH pattern, such as the NAO, the AMOC, and Greenland ice sheet melting, are also important in the generation of Atlantic cold blob events. These factors may weaken the apparent connection between the Pacific and Atlantic blobs. The connection can be better revealed if we focus on the TNH pattern and its associated oceanic covariability.

This study raises a number of unanswered questions. For example, what causes the TNH pattern to stay in its positive phase for an extended period of time? Previous studies have suggested the TNH (or TNH-like) pattern may be triggered by tropical forcing mechanisms, such as the El Niño (Mo and Livezey 1986; Barnston et al. 1991; Yu et al. 2012; Yu and Kim 2011; Yu and Zou 2013; Zou et al. 2014), the quasi-biennial oscillation (Barnston et al. 1991), the propagation of the wave activity initiated from the western tropical Pacific Ocean (Wang

et al. 2014; Lee et al. 2015; Seager and Henderson 2016; Hu et al. 2017), and the internal dynamics in the atmosphere (Kumar et al. 2013; Seager et al. 2014; Xie and Zhang 2017). Also, recent warming in the Arctic regions has been suggested to exert strong impacts on midlatitude weather and climate by altering large-scale atmospheric circulation patterns (Cohen et al. 2012, 2014; Kim et al. 2014; Peings and Magnusdottir 2014; Deser et al. 2015; Lee et al. 2015; Overland et al. 2015, 2016; Yu et al. 2017). Thus, forcing related to certain tropical Pacific Ocean or polar conditions may be potential factors for the phase-locking of the TNH pattern. Extensive investigations on the underlying dynamics of the TNH pattern are clearly warranted in future research, given its importance as a mechanism for connecting the climate of the North Pacific and Atlantic Oceans. In addition, we notice that the linear trends for the Pacific and Atlantic blob indices, when calculated using the nondetrended SST anomalies, are $0.007°C\,yr^{-1}$ and $-0.004°C\,yr^{-1}$, respectively. The trends, although small, may produce cumulative warming large enough to affect the characteristics of the Pacific and Atlantic blobs or their relationships with large-scale atmospheric circulation patterns in recent decades. This possibility also needs to be explored in the future.

REFERENCES

Alexander, M. A., I. Bladé, M. Newman, J. R. Lanzante, N.-C. Lau, and J. D. Scott, 2002: The atmospheric bridge: The influence of ENSO teleconnections on air–sea interaction over the global oceans. *J. Climate*, **15**, 2205–2231, doi:10.1175/1520-0442(2002)015<2205:TABTIO>2.0.CO;2.

Amaya, D. J., N. E. Bond, A. J. Miller, and M. J. DeFlorio, 2016: The evolution and known atmospheric forcing mechanisms behind the 2013-2015 North Pacific warm anomalies. *US CLIVAR Variations*, Vol. 14, No. 2, US CLIVAR, Washington, DC, 1–6, https://usclivar.org/newsletter/newsletters.

Barnston, A. G., and R. E. Livezey, 1987: Classification, seasonality and persistence of low-frequency atmospheric circulation patterns. *Mon. Wea. Rev.*, **115**, 1083–1126, doi:10.1175/1520-0493(1987)115<1083:CSAPOL>2.0.CO;2.

——, ——, and M. S. Halpert, 1991: Modulation of Southern Oscillation–Northern Hemisphere mid-winter climate relationships by QBO. *J. Climate*, **4**, 203–217, doi:10.1175/1520-0442(1991)004<0203:MOSONH>2.0.CO;2.

Behringer, D. W., M. Ji, and A. Leetmaa, 1998: An improved coupled model for ENSO prediction and implications for ocean initialization. Part I: The ocean data assimilation system. *Mon. Wea. Rev.*, **126**, 1013–1021, doi:10.1175/1520-0493(1998)126<1013:AICMFE>2.0.CO;2.

Bond, N. A., M. F. Cronin, H. Freeland, and N. Mantua, 2015: Causes and impacts of the 2014 warm anomaly in the NE Pacific. *Geophys. Res. Lett.*, **42**, 3414–3420, doi:10.1002/2015GL063306.

Bretherton, C. S., M. Widmann, V. P. Dymnidov, J. M. Wallace, and I. Bladé, 1999: The effective number of spatial degrees of freedom of a time-varying field. *J. Climate*, **12**, 1990–2009, doi:10.1175/1520-0442(1999)012<1990:TENOSD>2.0.CO;2.

Cohen, J., J. Furtado, M. Barlow, V. Alexeev, and J. Cherry, 2012: Arctic warming, increasing fall snow cover and widespread boreal winter cooling. *Environ. Res. Lett.*, **7**, 014007, doi:10.1088/1748-9326/7/1/014007.

——, and Coauthors, 2014: Recent Arctic amplification and extreme mid-latitude weather. *Nat. Geosci.*, **7**, 627–637, doi:10.1038/ngeo2234.

Delworth, T. L., F. Zenh, G. A. Vecchi, X. Yang, L. Zhang, and R. Zhang, 2016: The North Atlantic Oscillation as a driver of rapid climate change in the Northern Hemisphere. *Nat. Geosci.*, **9**, 509–512, doi:10.1038/ngeo2738.

Deser, C., R. A. Tomas, and L. Sun, 2015: The role of ocean–atmosphere coupling in the zonal-mean atmospheric response to Arctic sea ice loss. *J. Climate*, **28**, 2168–2186, doi:10.1175/JCLI-D-14-00325.1.

Di Lorenzo, E., and N. Mantua, 2016: Multi-year persistence of the 2014/15 North Pacific marine heatwave. *Nat. Climate Change*, **6**, 1042–1047, doi:10.1038/nclimate3082.

——, G. Liguori, and N. Mantua, 2016: Climate interpretation of the North Pacific marine heatwave of 2013-2015. *US CLIVAR Variations*, Vol. 14, No. 2, US CLIVAR, Washington, DC, 13–18, https://usclivar.org/newsletter/newsletters.

Duchez, A., D. Desbruyères, J. J.-M. Hirschi, E. Frajka-Williams, S. Josey, and D. G. Evan, 2016: The tale of a surprisingly cold blob in the North Atlantic. *US CLIVAR Variations*, Vol. 14, No. 2, US CLIVAR, Washington, DC, 19–23, https://usclivar.org/newsletter/newsletters.

Esbensen, S. K., 1984: A comparison of intermonthly and interannual teleconnections in the 700 mb geopotential height field during the Northern Hemisphere winter. *Mon. Wea. Rev.*, **112**, 2016–2032, doi:10.1175/1520-0493(1984)112<2016:ACOIAI>2.0.CO;2.

Franzke, C., and S. B. Feldstein, 2005: The continuum and dynamics of Northern Hemisphere teleconnection patterns. *J. Atmos. Sci.*, **62**, 3250–3267, doi:10.1175/JAS3536.1.

Gentemann, C. L., M. R. Fewings, and M. García-Reyes, 2017: Satellite sea surface temperatures along the West Coast of the United States during the 2014–2016 northeast Pacific marine heat wave. *Geophys. Res. Lett.*, **44**, 312–319, doi:10.1002/2016GL071039.

Hartmann, D., 2015: Pacific sea surface temperature and the winter of 2014. *Geophys. Res. Lett.*, **42**, 1894–1902, doi:10.1002/2015GL063083.

Henson, B., 2016: The North Atlantic blob: A marine cold wave that won't go away. WunderBlog, Weather Underground, https://www.wunderground.com/blog/JeffMasters/the-north-atlantic-blob-a-marine-cold-wave-that-wont-go-away.html.

Hu, Z.-Z., A. Kumar, B. Jha, J. Zhu, and B. Huang, 2017: Persistence and predictions of the remarkable warm anomaly in the northeastern Pacific Ocean during 2014–16. *J. Climate*, **30**, 689–702, doi:10.1175/JCLI-D-16-0348.1.

Jaffe, D. A., and L. Zhang, 2017: Meteorological anomalies lead to elevated O_3 in the western U.S. in June 2015. *Geophys. Res. Lett.*, **44**, 1990–1997, doi:10.1002/2016GL072010.

Johnstone, J. A., and N. J. Mantua, 2014: Atmospheric controls on northeast Pacific temperature variability and change, 1900–2012. *Proc. Natl. Acad. Sci. USA*, **111**, 14 360–14 365, doi:10.1073/pnas.1318371111.

Kalnay, E., and Coauthors, 1996: The NCEP/NCAR 40-Year Reanalysis Project. *Bull. Amer. Meteor. Soc.*, **77**, 437–471, doi:10.1175/1520-0477(1996)077<0437:TNYRP>2.0.CO;2.

Kim, B.-M., S.-W. Son, S.-K. Min, J.-H. Jeong, S.-J. Kim, X. Zhang, T. Shim, and J.-H. Yoon, 2014: Weakening of the stratospheric polar vortex by Arctic sea-ice loss. *Nat. Commun.*, **5**, 4646, doi:10.1038/ncomms5646.

Kumar, A., and Z.-Z. Hu, 2012: Uncertainty in the ocean-atmosphere feedbacks associated with ENSO in the reanalysis products. *Climate Dyn.*, **39**, 575–588, doi:10.1007/s00382-011-1104-3.

——, H. Wang, W. Wang, Y. Xue, and Z.-Z. Hu, 2013: Does knowing the oceanic PDO phase help predict the atmospheric anomalies in subsequent months? *J. Climate*, **26**, 1268–1285, doi:10.1175/JCLI-D-12-00057.1.

Lee, M.-Y., C.-C. Hong, and H.-H. Hsu, 2015: Compounding effects of warm sea surface temperature and reduced sea ice on the extreme circulation over the extratropical North Pacific and North America during the 2013–2014 boreal winter. *Geophys. Res. Lett.*, **42**, 1612–1618, doi:10.1002/2014GL062956.

Mantua, N. J., S. R. Hare, Y. Zhang, J. M. Wallace, and R. C. Francis, 1997: A Pacific decadal climate oscillation with impacts on salmon production. *Bull. Amer. Meteor. Soc.*, **78**, 1069–1079, doi:10.1175/1520-0477(1997)078<1069:APICOW>2.0.CO;2.

Medred, C., 2014: Unusual species in Alaska waters indicate parts of Pacific warming dramatically. *Alaska Dispatch News*, 14 September, http://www.adn.com/article/20140914/unusual-species-alaska-waters-indicate-parts-pacific-warming-dramatically.

Mo, K. C., 1985: Interhemisphere correlations statistics during the Northern Hemisphere winter. *Proc. Ninth Conf. on Probability and Statistics in Atmospheric Sciences*, Virginia Beach, VA, Amer. Meteor. Soc., 283–289.

——, and R. E. Livezey, 1986: Tropical-extratropical geopotential height teleconnections during the Northern Hemisphere winter. *Mon. Wea. Rev.*, **114**, 2488–2515, doi:10.1175/1520-0493(1986)114<2488:TEGHTD>2.0.CO;2.

Newman, M., G. P. Compo, and M. A. Alexander, 2003: ENSO-forced variability of the Pacific decadal oscillation. *J. Climate*,

16, 3853–3857, doi:10.1175/1520-0442(2003)016<3853:EVOTPD>2.0.CO;2.

Overland, J. E., J. A. Francis, R. Hall, E. Hanna, S.-J. Kim, and T. Vihma, 2015: The melting Arctic and midlatitude weather patterns: Are they connected? *J. Climate*, **28**, 7917–7932, doi:10.1175/JCLI-D-14-00822.1.

——, and Coauthors, 2016: Nonlinear response of mid-latitude weather to the changing Arctic. *Nat. Climate Change*, **6**, 992–999, doi:10.1038/nclimate3121.

Panagiotopoulos, F., M. Shahgedanova, and D. B. Stephenson, 2002: A review of Northern Hemisphere winter-time teleconnection patterns. *J. Phys. IV France*, **12**, 10–27, doi:10.1051/jp4:20020450.

Peings, Y., and G. Magnusdottir, 2014: Response of the wintertime northern hemisphere atmospheric circulation to current and projected Arctic sea ice decline: A numerical study with CAM5. *J. Climate*, **27**, 244–264, doi:10.1175/JCLI-D-13-00272.1.

Peng, P., and A. Kumar, 2005: A large ensemble analysis of the influence of tropical SSTs on seasonal atmospheric variability. *J. Climate*, **18**, 1068–1085, doi:10.1175/JCLI-3314.1.

Peterson, W., M. Robert, and N. Bond, 2015: The warm Blob continues to dominate the ecosystem of the northern California Current. *PICES Press*, Vol. 23, No. 2, North Pacific Marine Science Organization, Sidney, BC, Canada, 44–46, https://www.pices.int/publications/pices_press/volume23/PPJuly2015.pdf.

Rahmstorf, S., E. B. Jason, G. Feulner, M. E. Mann, A. Robinson, S. Rutherford, and E. J. Schaffernicht, 2015: Exceptional twentieth-century slowdown in Atlantic Ocean overturning circulation. *Nat. Climate Change*, **5**, 475–480, doi:10.1038/nclimate2554.

Rayner, N. A., D. E. Parker, E. B. Horton, C. K. Folland, L. V. Alexander, D. P. Rowell, E. C. Kent, and A. Kaplan, 2003: Global analyses of sea surface temperature, sea ice, and night marine air temperature since the late nineteenth century. *J. Geophys. Res.*, **108**, 4407, doi:10.1029/2002JD002670.

Robson, J., P. Ortega, and R. Sutton, 2016: A reversal of climatic trends in the North Atlantic since 2005. *Nat. Geosci.*, **9**, 513–517, doi:10.1038/ngeo2727.

Rogers, J. C., 1981: The North Pacific Oscillation. *J. Climatol.*, **1**, 39–57, doi:10.1002/joc.3370010106.

Schmittner, A., P. Bakker, R. L. Beadling, J. T. M. Lenaerts, S. Mernild, O. Saenko, and D. Swingedouw, 2016: Greenland ice sheet melting influence on the North Atlantic. *US CLIVAR Variations*, Vol. 14, No. 2, US CLIVAR, Washington, DC, 32–37, https://usclivar.org/newsletter/newsletters.

Schneider, N., and B. Cornuelle, 2005: The forcing of the Pacific decadal oscillation. *J. Climate*, **18**, 4355–4373, doi:10.1175/JCLI3527.1.

Seager, R., and N. Henderson, 2016: Tropical ocean forcing of the persistent North American west coast ridge of winter 2013/14. *J. Climate*, **29**, 8027–8048, doi:10.1175/JCLI-D-16-0145.1.

——, M. Hoerling, S. Schubert, H. Wang, B. Lyon, A. Kumar, J. Nakamura, and N. Henderson, 2014: Causes and predictability of the 2011–14 California drought. Assessment Rep., NOAA/OAR/Climate Program Office, 42 pp., http://cpo.noaa.gov/MAPP/californiadroughtreport.

——, ——, ——, ——, ——, ——, ——, and ——, 2015: Causes of the 2011–14 California drought. *J. Climate*, **28**, 6997–7024, doi:10.1175/JCLI-D-14-00860.1.

Siedlecki, S., E. Bjorkstedt, R. Feely, A. Sutton, J. Cross, and J. Newton, 2016: Impact of the Blob on the Northeast Pacific Ocean biogeochemistry and ecosystems. *US CLIVAR Variations*,

Vol. 14, No. 2, US CLIVAR, Washington, DC, 7–12, https://usclivar.org/newsletter/newsletters.

Swain, D. L., M. Tsiang, M. Haugen, D. Singh, A. Charland, B. Rajaratnam, and N. S. Diffenbaugh, 2014: The extraordinary California drought of 2013/2014: Character, context, and the role of climate change. *Bull. Amer. Meteor. Soc.*, **95** (Suppl.), S3–S7, doi:10.1175/1520-0477-95.9.S1.1.

——, D. E. Horton, D. Singh, and N. S. Diffenbaugh, 2016: Trends in atmospheric patterns conducive to seasonal precipitation and temperature extremes in California. *Sci. Adv.*, **2**, doi:10.1126/sciadv.1501344.

Wallace, J. M., and D. S. Gutzler, 1981: Teleconnections in the potential height field during the Northern Hemisphere winter. *Mon. Wea. Rev.*, **109**, 784–812, doi:10.1175/1520-0493(1981)109<0784:TITGHF>2.0.CO;2.

——, C. Smith, and C. S. Bretherton, 1992: Singular value decomposition of wintertime sea surface temperature and 500-mb height anomalies. *J. Climate*, **5**, 561–576, doi:10.1175/1520-0442(1992)005<0561:SVDOWS>2.0.CO;2.

Wang, S.-Y., L. Hipps, R. R. Gillies, and J.-H. Yoon, 2014: Probable causes of the abnormal ridge accompanying the 2013–2014 California drought: ENSO precursor and anthropogenic warming footprint. *Geophys. Res. Lett.*, **41**, 3220–3226, doi:10.1002/2014GL059748.

Whitney, F. A., 2015: Anomalous winter winds decrease 2014 transition zone productivity in the NE Pacific. *Geophys. Res. Lett.*, **42**, 428–431, doi:10.1002/2014GL062634.

Xie, J., and M. Zhang, 2017: Role of internal atmospheric variability in the 2015 extreme winter climate over the North America Continent. *Geophys. Res. Lett.*, **44**, 2464–2471, doi:10.1002/2017GL072772.

Xue, Y., B. Huang, Z.-Z. Hu, A. Kumar, C. Wen, D. Behringer, and S. Nadiga, 2011: An assessment of oceanic variability in the NCEP Climate Forecast System Reanalysis. *Climate Dyn.*, **37**, 2511–2539, doi:10.1007/s00382-010-0954-4.

Yeager, S. G., W. M. Kim, and J. Robson, 2016: What caused the Atlantic cold blob of 2015. *US CLIVAR Variations*, Vol. 14, No. 2, US CLIVAR, Washington, DC, 24–31, https://usclivar.org/newsletter/newsletters.

Yu, B., Z. W. Wu, and W. J. Merryfield, 2017: Relationship between North American winter temperature and large-scale atmospheric circulation anomalies and its decadal variation. *Environ. Res. Lett.*, **11**, 074001, doi:10.1088/1748-9326/11/7/074001.

Yu, J.-Y., and S. T. Kim, 2011: Relationships between extratropical sea level pressure variations and the central Pacific and eastern Pacific types of ENSO. *J. Climate*, **24**, 708–720, doi:10.1175/2010JCLI3688.1.

——, and Y. Zou, 2013: The enhanced drying effect of central-Pacific El Niño on US winter. *Environ. Res. Lett.*, **8**, 014019, doi:10.1088/1748-9326/8/1/014019.

——, ——, S. T. Kim, and T. Lee, 2012: The changing impact of El Niño on US winter temperatures. *Geophys. Res. Lett.*, **39**, L15702, doi:10.1029/2012GL052483.

Zaba, K. D., and D. L. Rudnick, 2016: The 2014–2015 warming anomaly in the Southern California Current System observed by underwater gliders. *Geophys. Res. Lett.*, **43**, 1241–1248, doi:10.1002/2015GL067550.

Zou, Y., J.-Y. Yu, T. Lee, M.-M. Lu, and S. T. Kim, 2014: CMIP5 model simulations of the impacts of the two types of El Niño on the U.S. winter temperature. *J. Geophys. Res. Atmos.*, **119**, 3076–3092, doi:10.1002/2013JD021064.